

Quantitative study of destructive quantum interference effect on the lin||lin CPT.

E. Breschi¹, G. Kazakov², R. Lammegger³, G. Mileti¹, B. Matisov², L. Windholz³

¹Laboratoire Temps-Fréquence - University of Neuchâtel,

Rue A.-L.-Breguet 1, 2000 Neuchâtel Switzerland

² St. Petersburg State Polytechnic University, Polytechnic str. 29, 195251 St.Petersburg Russia

³ Institute of Experimental Physics TU-Graz, Petersgasse 16 A-8010 Graz Austria

(Dated: May 28, 2019)

We investigate experimentally and theoretically the Coherent Population Trapping (CPT) effect occurring in ⁸⁷Rb D₁ line due to the interaction with linearly polarized laser light (lin||lin CPT). In this configuration the coherence has a quadrupol like nature and is strongly influenced by the hyperfine structure of the excited state; consequently the quantum interference between CPT states is an essential feature of this interaction scheme. We study the lin||lin CPT signal as a function of the laser optical detuning. The comparison between experimental and theoretical results allows us to quantify the contribution from different CPT states to the total signal. Based on these results we investigate the signal depending on both the pressure broadening of the optical transition and the laser linewidth, and we find in which conditions the laser linewidth does not degrade the amplitude of the lin||lin CPT.

PACS numbers: 42.50Gy, 42.62Fi, 32.10Fn

I. INTRODUCTION

The first investigations of the Coherent Population Trapping (CPT) effect were performed theoretically and experimentally in the seventies [1]. In accordance with these early works, the CPT effect is due to a coherence between ground states caused by the interaction with a quasi resonant, multi-frequency and coherent light field. CPT and related effects (such as Electromagnetically Induced Transparency [2] and Absorption [3]) have an impact on both, the atomic system state and the light beam propagation through the media.

Coherent Population Trapping resonances with a narrow linewidth can occur in the simplest case in quantum systems with two long-lived ground states and one excited state coupled by a bichromatic light field. The energy levels in such a configuration are arranged similar to the Greek letter Λ (so called Λ -System) and can be found, for instance, in alkali atoms. The properties of the CPT resonance can be exploited in a wide range of applications such as atomic magnetometry [4], atomic frequency standards [5], pulse delaying and compression for optical memory [6].

The problem in the use of CPT effect in those applications is the low resonance amplitude. To obtain higher resonance amplitude and minimum linewidth of CPT resonances, recently several novel light-atom interaction schemes were proposed [7, 8]. In particular in work [9] the authors showed that a significant enhancement of the CPT amplitude can be obtained in the so-called lin||lin CPT configuration. Here two co-propagating linearly polarized laser waves with parallel linear polarization vectors are resonant with the transitions to $5^2P_{1/2}$ $F_e = 1$ of the ⁸⁷Rb isotope. A detailed analysis of the two photon absorption process by choosing a second order perturbative approach has shown that in a lin||lin CPT configuration the coupling has quadrupol like ($K=2$) nature [10]. The consequence is that the strength of lin||lin

CPT-resonances depends critically on the excited state hyperfine structure (hfs) in a way different to that of the well known CPT resonances obtained by a circularly polarized laser field [11].

A theoretical study of a four-level system describing different double-CPT resonance features depending on the structure of the ground and excited atomic levels has been published in [12]. The interest of these systems relies to the possibility of controlling its optical properties via the quantum interference arising between two dark states, for instance, by means of the phases of the laser fields [13, 14] or the local phase of the CPT states [15]. In the present work we study the behavior of the lin||lin CPT configuration occurring within the manifold of hyperfine (hf) transitions within the D₁ line of ⁸⁷Rb. In our case the multi-CPT feature depends on the structure of the excited hyperfine states and it is described in detail in section II with the model developed for the data interpretation. We analyze the lin||lin CPT signal depending on the laser detuning and the homogeneous broadening (in section IV), which depends on the pressure broadening (due to the buffer gas in the cell) and the laser linewidth. Note that the evaluation of the laser linewidth influence on the CPT is crucial for applications and has not been investigated much so far. A theoretical study of the laser linewidth effects on CPT for achieving selective excitation of atoms (with application in laser cooling and quantum computing) is presented in reference [16]; while in [17] the author has demonstrated with his model a scheme that allows large time delay for large bandwidth optical pulse.

We study lin||lin CPT signals obtained with two different light sources: a pair of Phase-Locked (PL) Extended Cavity Diode Lasers (ECDLs) and a current modulated Vertical Cavity Surface Emitting Laser (VCSEL). The PL lasers have, in good approximation, a pure bichromatic fields with a narrow linewidth. On the contrary, the modulated VCSEL has a multi-frequency spectrum

with broader linewidth. A detailed discussion of the laser sources and of the experimental setup is presented in section III.

II. MODEL AND INTERACTION SCHEME

A model based on the density matrix approach has been used for the data interpretation and has been described in detail in reference [18]. Here we briefly report on the basic approach and we give an intuitive picture of the results essential for our discussion.

Let us to consider a ^{87}Rb atom excited by a two-frequency laser field resonant to the hyperfine transitions $5^2S_{1/2} F_g = 1, 2 \leftrightarrow 5^2P_{1/2} F_e = 1$ of the D_1 line. For such a system the density matrix evolution is given by

$$\dot{\rho}_{ij} = -\frac{i}{\hbar} \sum_k [H_{ik} \rho_{kj} - \rho_{ik} H_{kj}] + \sum_{k,l} \Gamma_{ij,kl} \rho_{kl}. \quad (1)$$

The Hamiltonian is denoted by \hat{H} separated in an atomic unperturbed Hamiltonian \hat{H}_0 and an interaction operator \hat{V} , i.e. $\hat{H} = \hat{H}_0 + \hbar\hat{V}$. The two frequency laser field is described by

$$\vec{E}(z, t) = \sum_{j=1,2} \left[\frac{\vec{E}_j}{2} \exp[i(\omega_j t + \varphi_j(t) - k_j z)] + c.c. \right], \quad (2)$$

whereas the laser line width is modeled by the phase fluctuations $\varphi_j(t)$. Finally in equation (1) the relaxation processes are described by the relaxation matrix element $\Gamma_{ij,kl}$.

At high temperature an optical absorption cell (as used in the experiments) becomes optically thick. As a consequence the density matrix elements (and with it the CPT signal) are functions of the light intensity along the optical path. The density matrix elements by themselves are influencing the absorption and the dispersion properties of the medium. Modeling of such a coupled behavior is rather complicated because, strictly speaking, the effects of propagation determined by the Maxwell equations are strongly coupled with the density matrix equations of the quantum system. Therefore in our model the optical path is divided in a set of subsequent parts. Assuming constant electrical (E) fields in each thin layer the density matrix is calculated. Finally the Maxwell equations for the slowly varying E-field amplitude and phase [19], are used to calculate the variations of the E-fields within the layer. Thereafter the density matrix of the next layer is determined by using the new E-field derived from the previous layer. This procedure is repeated for all subsequent parts.

However in the numerical calculations we don't take into account modifications of the transverse intensity distribution. Nevertheless, this simple phenomenological approach allows us to reproduce the experimental results (see Fig. 5).

In the following the ground and excited state Zeeman sublevels are called g , g' and e , respectively. Note that g and g' belong to different hyperfine ground states and a CPT state can be created when the two transitions, $|g\rangle \leftrightarrow |e\rangle$ and $|g'\rangle \leftrightarrow |e\rangle$, are excited simultaneously.

If the laser field intensity is much lower than the saturation limit for each optical transition, the total excited state population ρ_{exc} is proportional to the light power absorbed and is related to the ground state density matrix through the equation

$$\rho_{exc} = \sum_{e,g,g'} \left[\frac{V_{eg}^0 V_{g'e}}{\gamma' \gamma} (G_{ge} + G_{g'e} + i(F_{ge} - F_{g'e})) \rho_{gg'} \right]. \quad (3)$$

The ground state density matrix itself can be found from the following set of equations:

$$\begin{aligned} \dot{\rho}_{gg'} = & -i\rho_{gg'}(\omega_{gg'} - \omega_g + \omega_{g'}) + \Gamma\left(\frac{\delta_{gg'}}{8} - \rho_{gg'}\right) - \\ & \sum_{g'',e} \left[\frac{V_{ge} V_{eg''}}{\gamma'} (G_{g'} + iF_{g'e}) \right] \rho_{g''g'} - \\ & \sum_{g'',e} \left[\frac{V_{g''e} V_{eg'}}{\rho} \gamma'_{gg''} (G_{ge} - iF_{ge}) \right] + \delta_{gg'} \times \\ & \left. \sum_{e,g'',g'''} \left[\frac{V_{g''e} V_{eg''''}}{\gamma'} (G_{g''e} + G_{g''e} + i(F_{g''''e} - F_{g''e})) \right] \right]. \end{aligned} \quad (4)$$

$$\sum_g \rho_{gg} = 1. \quad (5)$$

Here $\hbar V_{ij}$ are the matrix elements of the interaction Hamiltonian in the rotating frame (Rabi frequencies); γ is the excited state decay rate; γ' is the decay rate of the optical coherence ρ_{eg} ; $\delta_{gg'}$ is the Kronecker delta. Γ is the ground state relaxation rate determined by the temperature of the cell, type and pressure of buffer gas, geometry of the cell and laser beam [20]; ω_g is the frequency of the laser component interacting with the level g ; and $\omega_{gg'}$ is the frequency spacing between the levels $|g\rangle$ and $|g'\rangle$.

In [21], the authors demonstrate that the optical coherence decay rate γ' is determined by the laser linewidth Γ_L , by the spontaneous relaxation rate γ_{sp} which is for Rubidium $\simeq 2\pi \cdot 5.6$ MHz, and by the pressure broadening γ_c which depends on the type of buffer gas and on the buffer gas pressure in the cell:

$$\gamma' = \frac{\gamma_{sp} + \gamma_c + \Gamma_L}{2}. \quad (6)$$

To understand the physical meaning of γ' let us consider a generic single transition $|g\rangle \leftrightarrow |e\rangle$. The excitation of this transition by a laser light field of linewidth Γ_L , results in an homogeneous broadened profile that can be described with a Lorentzian curve of linewidth γ' (figure 1).

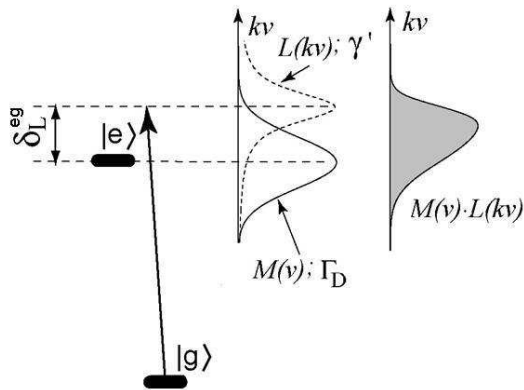


FIG. 1: Schematic view of the homogeneous broadening profile (Lorentzian curve $L(kv)$ of linewidth γ' in dashed line), of a transition ($|g\rangle \leftrightarrow |e\rangle$). δ_L^{eg} is the laser detuning. The Gaussian curve (of linewidth Γ_D) in solid line, represents the Doppler profile $M(v)$ of the transition. In equation (7) G_{ge} is proportional to the grey area under the product of the two curves ($L(kv) \cdot M(v)$).

The coefficients G_{ge} and F_{ge} in equation 3 and 4 are real and equal to:

$$G_{ge} = \int_{-\infty}^{+\infty} \frac{(\gamma')^2 M(v)}{(\gamma')^2 + (\delta_L^{eg} - kv)^2} dv,$$

$$F_{ge} = \int_{-\infty}^{+\infty} \frac{\gamma'(\delta_L^{eg} - kv)M(v)}{(\gamma')^2 + (\delta_L^{eg} - kv)^2} dv, \quad (7)$$

where $M(v)$ is the atomic velocity distribution and δ_L^{eg} is the laser detuning.

The coefficient G_{ge} is proportional to the strength of the single optical transition $|g\rangle \leftrightarrow |e\rangle$; while the coefficient F_{ge} allows to calculate the shift of the resonance frequency. For our intent we focus our attention to the coefficient G_{ge} which is schematically represented in figure 1. G_{ge} is proportional to the grey area delimited by the product of two profiles: the Doppler profile, represented by a Gaussian curve $M(v)$ of linewidth Γ_D , and the homogeneous profile, represented by a Lorentzian curve $L(kv)$ of linewidth γ' . If there is the possibility of a multi-channel excitation, G_{ge} characterizes the contribution of each transition to the total excitation process.

Now we extend the previous consideration made for a single optical transition to a CPT state. The necessary condition for creating the CPT state is that the transitions from both ground states $|g\rangle$ and $|g'\rangle$ towards the same excited level $|e\rangle$ are simultaneously excited. The straightforward consequence is that the one-photon detuning of both light field components must coincide ($\delta_L^{eg} = \delta_L^{eg'}$). Under this condition, from equation 7 the relation $G_{ge} = G_{g'e} = G_e$ can be derived. In synthesis the G-coefficient for a general CPT state depends only on the excited states involved (and not on the ground states). When multi-CPT resonances take part, the con-

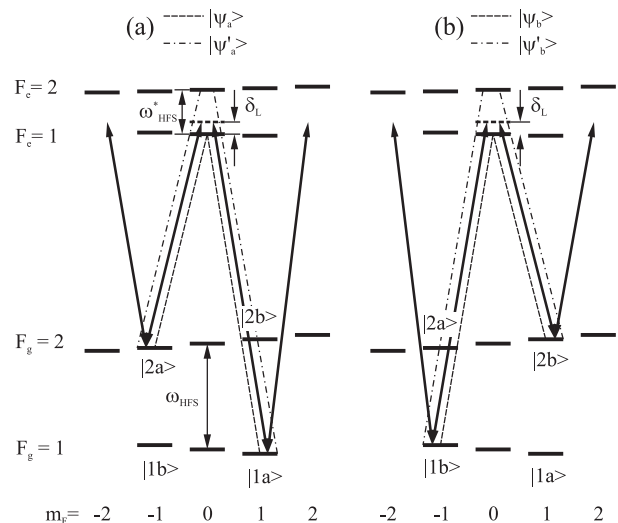


FIG. 2: Schematic diagram of the light induced transitions giving the lin||lin CPT signal from the levels: $|1a\rangle = |F_g = 1, m_F = +1\rangle$ and $|2a\rangle = |F_g = 2, m_F = -1\rangle$ part (a) of the figure; $|1b\rangle = |F_g = 1, m_F = -1\rangle$ and $|2b\rangle = |F_g = 2, m_F = +1\rangle$ part (b) of the figure. In presence of a low magnetic field along the laser propagation direction (= quantization axis) the CPT states in (a) and (b) are degenerate. The solid arrows are representing the components of the exciting laser field. For simplicity δ_L represents the laser detuning.

tribution to the total signal of each single CPT state can be characterized by calculating G_e .

Our model takes into account the Zeeman and hyperfine structure of the ^{87}Rb atoms. In the following we define the interaction scheme, i.e. which group of atomic sublevels are involved in the CPT formation. We present the results obtained by applying the model to an isolated reduced system, in order to show how the G_i coefficients describe the CPT resonance amplitude.

Figure 2 shows the relevant transitions induced by the coherent σ^+ and σ^- components of the linearly polarized light fields expressed in spherical tensor basis. In figure 2 we do not report the $\sigma^+ - \sigma^+$ and $\sigma^- - \sigma^-$ groups of transitions, because the CPT states arising from these groups forms closed-loop systems. In general, the existence of CPT is directly connected with the phase relation between the Rabi frequencies (phase relation of laser fields and atomic wave functions) along the excitation contour [13]. In the specific case the $\sigma^+ - \sigma^+$ and $\sigma^- - \sigma^-$ CPT resonances interfere destructively and do not contribute to the total lin||lin CPT signal at $\omega \approx \omega_{hfs}$ [7]. We study the $\sigma^+ - \sigma^-$ CPT resonances between ground state Zeeman sublevels with $m_F = \pm 1$. The feature of the multi-CPT is related with the presence of two excited levels ($F_e=1,2$), both allowed for dipole transitions.

Finally four CPT states contribute to the total lin||lin CPT resonance at $\omega \approx \omega_{hfs}$: $|\Psi_a\rangle$ and $|\Psi_b\rangle$ are the coherent superpositions of the Zeeman sublevels $|1a\rangle \leftrightarrow |2a\rangle$ and $|1b\rangle \leftrightarrow |2b\rangle$ through the excited state $F_e = 1$, while

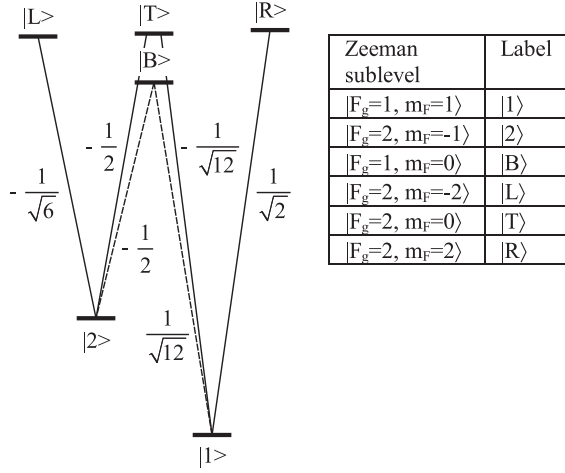


FIG. 3: Isolated 6-level excitation system. The coefficients reported near the transition are proportional to the Rabi frequencies V_{eg} , i.e. they are the dipole matrix element for the transitions expressed as multiples of the coefficient $V^0 = \sqrt{\frac{3\gamma_{sp}c^3\hbar}{2\omega^3}}$.

$|\Psi'_a\rangle$ and $|\Psi'_b\rangle$ are the coherent superpositions of the same Zeeman sublevels via the excited state $F_e = 2$. When a magnetic field is applied along the quantization axis $|\Psi_a\rangle$ - $|\Psi_b\rangle$ and $|\Psi'_a\rangle$ - $|\Psi'_b\rangle$ split with a factor of ± 28 Hz/ μ T determined by the nuclear g-factor. Remark that the transitions towards the outermost Zeeman sublevels $|F_e = 2, m_F = \pm 2\rangle$, play an important role in the formation of the CPT state $|\Psi'_a\rangle$ and $|\Psi'_b\rangle$, and thus in the total lin||lin CPT signal.

A. Simplified atomic system: analytical solution

To point out how the G_i coefficient can describe the total lin||lin CPT signal we apply the approach presented at the beginning of this section to figure 2 (a), under the hypothesis that the 6 levels participating to the interaction are isolated. Similar considerations can be applied to figure 2 (b) and then to the total lin||lin CPT signal. Figure 3 is the diagram of the isolated 6-level system. The Zeeman sublevels are named with a short label for handling with a compact notation. The coefficients reported near each transition are the dipole matrix elements expressed as multiples of $V^0 = \sqrt{\frac{3\gamma_{sp}c^3\hbar}{2\omega^3}}$. These coefficients are proportional to the Rabi frequencies, V_{eg} [22, 23]. For instance, in our notation the Rabi frequency for the transition $|1\rangle \leftrightarrow |R\rangle$ is named V_{1R} and is equal to $(\frac{1}{\sqrt{2}} \cdot V^0 \cdot \frac{E_1^+}{2\hbar})$, where E_1^+ is the cyclic projection of $\vec{E}1$ (equation 2).

There are only two ground state levels $|1\rangle$ and $|2\rangle$ in our simplified scheme, therefore the normalization condition (5) gives $\rho_{11} + \rho_{22} = 1$. We introduce for simplicity the new variables: f (population difference), R and J (real

and imaginary part of ρ_{12}):

$$\rho_{11} = (1+f)/2, \quad \rho_{22} = (1-f)/2, \quad \rho_{12} = R + i \cdot J. \quad (8)$$

The total excited state population ρ_{exc} can be obtained by applying equation (3):

$$\rho_{exc} = \frac{1}{\gamma} [W + (W_1 - W_2) \cdot f + 4W_{12} \cdot R]. \quad (9)$$

From equations (4) and (8), we obtain the set of equations for variables f , R and J :

$$\begin{aligned} \dot{f} &= -(\Gamma + W) \cdot f - 4D_{12} \cdot J + W_2 - W_1, \\ \dot{R} &= -(\Gamma + W) \cdot R + (\Omega - \Delta) \cdot J - W_{12}, \\ \dot{J} &= D_{12} \cdot f - (\Gamma + W) \cdot J - (\Omega - \Delta) \cdot R. \end{aligned} \quad (10)$$

Here $\Omega = (\omega_2 - \omega_1 - \omega_{21})$ is the Raman detuning and Γ is ground state relaxation rate,

$$W_1 = \frac{|V_{1B}|^2}{\gamma'} G_1 + \frac{|V_{1T}|^2 + |V_{1R}|^2}{\gamma'} G_2, \quad (11)$$

$$W_2 = \frac{|V_{2B}|^2}{\gamma'} G_1 + \frac{|V_{2T}|^2 + |V_{2L}|^2}{\gamma'} G_2, \quad (12)$$

$$W = W_1 + W_2, \quad (13)$$

$$W_{12} = \frac{V_{1B}V_{B2}}{\gamma'} G_1 + \frac{V_{1T}V_{T2}}{\gamma'} G_2, \quad (14)$$

$$D_{12} = \frac{V_{1B}V_{B2}}{\gamma'} F_1 + \frac{V_{1T}V_{T2}}{\gamma'} F_2, \quad (15)$$

$$\Delta = \frac{|V_{2B}|^2 - |V_{1B}|^2}{\gamma'} F_1 + \frac{|V_{2T}|^2 + |V_{2L}|^2 - |V_{1T}|^2 - |V_{1R}|^2}{\gamma'} F_2. \quad (16)$$

Substituting the stationary solution of the set of equations (10) into (9), we obtain the following analytical expression for the total excited state population:

$$\rho_{exc} = \left[W - \frac{(W_1 - W_2)^2 + 4W_{12}^2}{\Gamma + W} + \frac{4(D_{12}(W_1 - W_2) - W_{12}(\Omega - \Delta))^2}{(\Gamma + W)((\Gamma + W)^2 + 4D_{12}^2 + (\Omega - \Delta)^2)} \right] \quad (17)$$

The first two terms in (17) do not depend on the two-photon detuning Ω ; the third term gives the change in the absorption due to the CPT effect. Finally, we substitute the Rabi frequencies (V_{eg}) into (11), (12) and (14) and we get:

$$W_1 = \frac{|V^0|^2}{\gamma'} \left[\frac{1}{12} G_1 + \frac{7}{12} G_2 \right], \quad (18)$$

$$W_2 = \frac{|V^0|^2}{\gamma'} \left[\frac{3}{12} G_1 + \frac{5}{12} G_2 \right], \quad (19)$$

$$W_{12} = \frac{|V^0|^2}{\gamma'} \frac{G_2 - G_1}{4\sqrt{3}}, \quad (20)$$

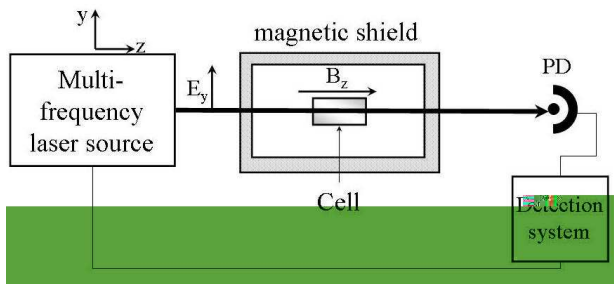


FIG. 4: Block diagram of the experimental setup. The multi-frequency excitation light has been generated by using two phase-locked ECDLs or by modulating a VCSEL. The photo-detector signal can be directly monitored by a digital oscilloscope and/or sent to a double-phase lock-in amplifier.

When $G_1 = G_2$, the two terms ($W_1 - W_2$) and W_{12} are vanishing, therefore the third term in 17 is vanishing, and the CPT amplitude goes to zero. This is an evidence of destructive quantum interference between the different CPT excitation channels (via the two excited state hyperfine sublevels).

III. EXPERIMENTAL SETUP

The sketch of the experimental setup is shown in figure 4. The core is a glass cell with a volume of a few cm^3 containing the ^{87}Rb isotope and N_2 as buffer gas. The cell temperature during the experiments was stabilized to $(68 \pm 1)^\circ\text{C}$, corresponding to a Doppler broadening of the optical transitions of $\Gamma_D = 2\pi \cdot 540$ MHz. Since the light fields are both co-propagating the Doppler broadening of the CPT resonance is due to the 6.8 GHz difference frequency. However - in the case of CPT in a buffered cell - the microwave Doppler effect is strongly reduced by the Dicke narrowing [24] because the atoms are confined within a volume of much smaller than the 4.4 cm wavelength corresponding to the 6.8 GHz frequency.

In order to avoid the influence of spurious magnetic fields and magnetic gradients, the cell was inserted in a CO-NETIC alloy magnetic shield. Inside the shielding, a solenoid provided the longitudinal magnetic field, $B_z = (3.0 \pm 0.2) \mu\text{T}$. The magnetic field has been regularly monitored during the experiments by using the g_J dependence of the outermost CPT signal [9], i.e. the CPT states created by the coherence of $|F_e = 1, m_F = 0\rangle$ and $|F_e = 2, m_F = \pm 2\rangle$.

The relevant spectral characteristics of the two laser systems used in our experiments are described in the following.

Modulated VCSEL (see ref [25]): The injection current of a single mode VCSEL emitting at 795 nm, is directly modulated with 3.417 GHz (i.e. half of the ground state hyperfine separation in ^{87}Rb). The linewidth of the VCSEL is about 100 MHz, measured from hetero-

dyne beatnote. The VCSEL modulation performance has been evaluated through the one-photon ^{87}Rb absorption spectrum by changing the frequency and the amplitude of the current modulation. We did not notice any influence of amplitude modulation, and the frequency modulation index was evaluated to be about 1.8. Under these conditions about 68% of the total laser power is contained in the first-order side-bands which are used for CPT preparation. The remaining 32% of the total power is distributed among mainly the carrier frequency and the higher-order side-bands. These off-resonant parts of the VCSEL-spectrum are causing one-photon excitation processes because of the Doppler broadening of the hyperfine transitions and are acting as loss mechanisms for the lin||lin CPT. Additionally, the not absorbed off-resonant light is increasing the dc and shot noise level of the photo-detector.

Phase-Locked (PL) lasers: The PL lasers are based two Extended Cavity Diode Lasers (ECDLs), a master and a slave laser. The master laser is stabilized to the ^{87}Rb D₁ line $5^2\text{S}_{1/2} F_g = 2 \rightarrow 5^2\text{P}_{1/2} F_e = 1$ transition, using an auxiliary evacuated ^{87}Rb cell in a DF-DAVLL [26]. The master laser has a linewidth of 0.5 MHz which is reduced to 0.04 MHz with high speed servo electronics. The light beams from the master and the slave ECDL are superimposed on a fast photodiode which detects the 6.8 GHz beat required for CPT experiments. After amplification, the beat signal is down converted in a double balanced ring mixer to 50 MHz and is compared to a reference frequency signal from an Intermediate Frequency (IF) oscillator. A digital phase/frequency detector provides an output signal proportional to the phase difference between the down converted beat-note and the IF-Oscillator. In this setup the advantages of an analogue (low phase noise) and a digital phase detector (high stability and large capture range) are combined, avoiding laser phase excursions that can lead to a destruction of the coherence [27]. In the case of PL lasers, the frequency components of the bichromatic electromagnetic field used in the CPT-experiments are separated by 6.835 GHz. The intensities as well as the linear polarization state are selected to be the same for both frequencies. Finally, to avoid a residual broadening of the CPT-resonances due to a wave vector mismatch, a polarization maintaining single mode fibre is used to ensure perfect collinear wave vectors of the two frequency components.

IV. MULTI-CPT STRUCTURE INFLUENCE ON THE LIN||LIN CPT AMPLITUDE

The influence of the excited state hyperfine structure of the ^{87}Rb D₁ line is evidenced by studying the lin||lin CPT signal versus the laser detuning (δ_L) in a cell containing ^{87}Rb and N_2 as buffer gas, $P_{\text{N}_2} = 0.5$ kPa. The collisional broadening γ_c at this pressure is about $2\pi \cdot 70$ MHz [28], i.e. γ_c is almost 12 times smaller than the splitting of the hyperfine excited states ($\omega_{hfs}^* = 2\pi \cdot 817$ MHz).

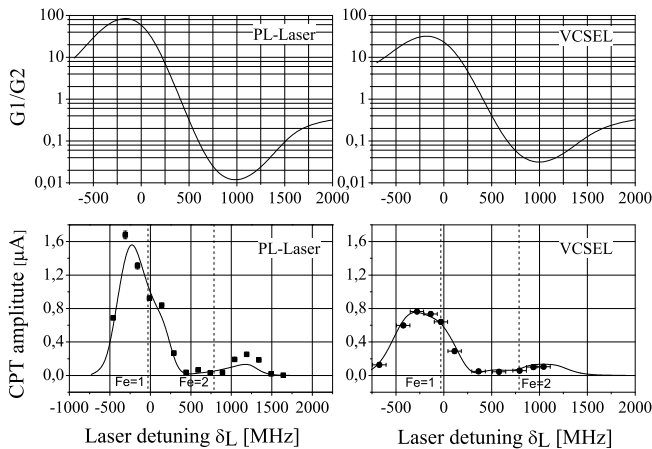


FIG. 5: The lower plots show the dependence of CPT amplitude versus laser detuning (δ_L) for the cell with $P_{N_2} = 0.5$ kPa; while in the upper plots the G_1/G_2 ratio calculated for the two set of data, are reported. $\delta_L = 0$ is defined with respect to an evacuated cell and the maximum of absorption in the cell is marked by the dotted vertical line (the pressure shift is about -30 MHz). In both cases, A_C goes to zero when $(G_1/G_2) = 1$ and has two maxima at the maximum and the minimum of (G_1/G_2) , respectively. Remark that the maxima of A_C are shifted with respect to the maxima of absorption in the cell.

As a consequence the hyperfine excited state structure is resolved.

These measurements can be easily performed with a modulated VCSEL since the VCSEL output frequency can be tuned with injection current over a wide frequency range (more than ten GHz). The situation is different for the PL lasers which are based on two ECDLs. In this case it is necessary to provide a frequency reference for each value of δ_L . The problem was solved by combining two techniques: the Saturation Absorption (SA) spectrum from a single arm of the DF-DAVLL setup provides an absolute reference over the ^{87}Rb D₁ line. Moreover a part of the master laser beam is sent through a confocal Fabry Perot interferometer with a Free Spectral Range of $\text{FSR} = 149.85$ MHz. The two signals (SA and Fabry Perot peaks) are measured simultaneously by an oscilloscope. In this way the master laser frequency output can be swept over the SA spectrum with the step determined by the Fabry Perot FSR. The slave laser was phase-locked to the master, ensuring good phase-locking condition even with the free-running master laser. The linewidth of the PL lasers working with un-locked laser is 0.5 MHz. During the measurements the reference signal was monitored regularly to control the Fabry Perot drift, which determine the uncertainty on the δ_L values.

The dependence of the lin||lin CPT amplitude (A_C) on δ_L is shown in the lower plots of figure 5, for experiments performed with PL lasers and modulated VCSEL, respectively. In figure 5 the points are the results of the

experiments while the solid lines are the model results. To quantify the influence of the each single CPT resonance contributing to the total lin||lin CPT signal, in section II the coefficient G_e have been introduced. In the two upper plots of figure 5, the calculated (G_1/G_2) values are reported as a function of the laser detuning for the two sets of data. In each plot $\delta_L = 0$ refers to the unperturbed group of transitions toward $F_e = 1$ (evacuated cell); and the dotted lines represent the maxima of absorption for $F_e = 1$ ($\delta_L \approx -30$ MHz) and $F_e = 2$ ($\delta_L \approx 787$ MHz) in the cell containing $P_{N_2} = 0.5$ kPa (collisional shift is (-22.2 ± 0.4) GHz K (kPa)⁻¹ [28]). For each laser system, we observe that A_C shows two relative maxima which are both shifted with respect to the two maxima of absorption in the cell. In particular the maxima of A_C coincide with the maximum and the minimum value of (G_1/G_2) , respectively. Note that in general the CPT state $|\Psi'_a\rangle$ is affected by the losses due to the one-photon transitions towards to the outermost excited levels $5^2P_{1/2}$ $F_e = 2$, $m_F = \pm 2$ (see figure 2). For this reason when $(G_1/G_2) < 1$ the resulting lin||lin CPT signal is smaller than the one for $(G_1/G_2) > 1$. The values of A_C dramatically decrease when the light sources (PL lasers and VCSEL) are tuned between the two groups of transitions. In fact we showed that both CPT excitation channels via different excited hyperfine sublevels interfere destructively, and, if their involvements into excitation process are equal, i.e. $G_1/G_2 = 1$, the CPT resonance vanishes. Moreover, by comparing the left and right part of figure 5, we can observe that the A_C maximum recorded in the experiments using PL lasers is larger than the A_C maximum obtained with the modulated VCSEL. This behaviour is well reproduced by the model. In particular it is worth to notice that - at the experimental conditions referring to figure 5 - the G_e coefficients calculated for PL lasers are bigger than these coefficients calculated for the modulated VCSEL, either for $e = 1$ and 2.

A. lin||lin CPT amplitude versus homogeneous broadening

The previous results allow us to predict the influence of the homogeneous broadening γ' (equation 6) on the lin||lin CPT signal. In practice we compare the experiments performed with PL lasers and modulated VCSEL in ^{87}Rb cells containing different pressures of N_2 for a fixed value of the laser detuning. In particular we discuss the case of detuning $\delta_L = 0$, when the master laser of PL lasers is stabilized, allowing the optimal performances of the system: the PL lasers linewidth Γ_P is 0.04 MHz, i.e. it is roughly 10^3 times narrower than the VCSEL linewidth ($\Gamma_V \approx 100$ MHz). Figure 6 shows the lin||lin CPT amplitude (A_C) versus the resonant laser power for two cells containing buffer gas with pressure $P_{N_2} = 0.5$ and 1.5 kPa, figure 6 (a) and (b), respectively. The main difference between the experiments in the two

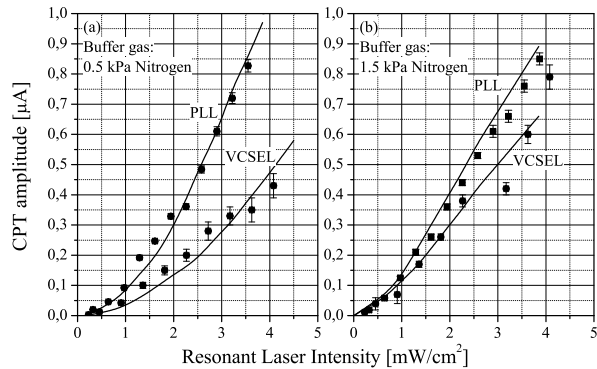


FIG. 6: Dependence of lin||lin CPT amplitude (A_C) versus the resonant laser power for experiments performed in two cells such as $P_{N_2} = 0.5$ (a) and $P_{N_2} = 1.5$ kPa (b). The solid points refer to experiments and the lines show the theoretical results. Remark that in (a) there is a noticeable difference in A_C depending on the laser source, while in (b) that difference is reduced.

cells is the relation between the collisional broadening in each cell and the VCSEL linewidth. For $P_{N_2} = 0.5$ kPa, the collisional broadening contribution $\gamma_c = 2\pi \cdot 70$ MHz is smaller than the linewidth of the VCSEL ($\gamma_c < \Gamma_V$). On the contrary, for $P_{N_2} = 1.5$ kPa, γ_c is $2\pi \cdot 210$ MHz, i.e. about 2 times Γ_V . Note that γ_c in both cases (cell with 0.5 and with 1.5 kPa of N_2) is much bigger than the PL laser linewidth ($\gamma_c \gg \Gamma_P$). In figure 6 (a) and (b) the solid points refer to the experiments performed with the modulated VCSEL and the PL lasers, respectively. The solid lines show the results of the theoretical model, and are in good quantitative agreement with the experimental results. We observe that the difference in A_C obtained with the two laser systems is large in (a) while it is reduced, and almost negligible, for $P_L < 1$ mW cm $^{-2}$, in (b). To explain the observed behaviour we first note that in reference [25] the authors showed a reduction of the CPT amplitude when the laser linewidth is larger than the pressure broadening for the CPT states created via the interaction with circularly polarized laser light. They explained this results by considering that the CPT resonance is excited in atoms belonging to several velocity classes. This argument is still valid, of course, in the case of lin||lin CPT signal, but can only partially explain our results. In fact, the CPT states obtained by interactions with linearly and circularly polarized light have different polarity, therefore they are intrinsically different. In the case of circularly polarized light fields, the CPT states

arise from a vectorial coupling and no quantum interference between two CPT states can occur [10]. In the previous parts of this communication we have demonstrated that in the case of CPT state arising from a quadrupolar coupling the excited state hyperfine structure must be taken into account for each δ_L . Under quadrupolar coupling conditions the phase relations of all Rabi frequencies, involved within the excitation scheme, plays a major role. Using the formalism developed in our model, we can conclude that for intensity lower than the saturation of the optical transitions, when $\gamma_c > \Gamma_L$ (condition satisfied in figure 6 (b)), it is possible to obtain the same (G_1/G_2) ratio for the two laser systems, i.e. it is possible to find experimental conditions in which the amplitude of the total lin||lin CPT signal, A_C , is independent of the laser linewidth. On the contrary, when $\gamma_c < \Gamma_L$ (condition satisfied in figure 6(a)), the laser linewidth plays an important role in the multi-CPT excitation; i.e. the ratio (G_1/G_2) is smaller than (G_1/G_2) for the PL lasers.

V. CONCLUSIONS

We present a study of lin||lin CPT, focusing our attention to the signal between ground state Zeeman sublevels such as $m_F = \pm 1$. This interaction scheme is characterized by a multi-CPT structure and by quantum interference between CPT states prepared through the two excited hyperfine states. A model is developed taking into account the multi-level structure of the atomic system and the multi-frequency spectrum of the light sources. We study the signal as a function of the laser detuning, i.e. the excited state hyperfine structure. By comparing the model and the experimental results we can quantify the influence of each CPT state on the total lin||lin CPT signal. Finally the good quantitative agreement between theory and experiments allows predicting the effects of the laser linewidth on the lin||lin CPT signal.

VI. ACKNOWLEDGMENTS

We are grateful to Prof. Pierre Thomann for the stimulating discussion. The work is supported by the INTAS-CNES grant 06-100024-9321, by the the Fund for Non-Profit 'Programs Dinastiya', by the Swiss National Research Foundation (SNRF grant. 200020-118062), and by the Austrian Science Found (FWF) (Project L300N02:A dark state Magnetometer)

[1] K. Takagi , R. F. Curl , R. T. M. Su, Appl. Phys., **7**,(1975) 298. G. Alzetta, A. Gozzini, M. Moi, G. Orriols, Nuovo Cimento B **36**, 5 (1976). E. Arimondo, G.

Orriols, Nuovo Cimento Lett., **17**, 333 (1976).

[2] S. E. Harris, Phys. Today **50**, 7 (1997).

[3] A. Lezama, S. Barreiro, A. M. Akulshin, Phys. Rev. A

- 59** 4732 (1999).
- [4] A. Nagel, K. Graf, A. Naumov, E. Mariotti, V. Biancalana, D. Meschede, R. Wynands, *Europhys. Lett.* **44**, 31 (1998).
- [5] J. Vanier, *Appl. Phys. B*, **81** 421442 (2005).
- [6] L. V. Hau, S. E. Harris, Z. Dutton, C. H. Behroozi, *Nature* **397**, (1999) 594. G. P. Djotyan, *Opt. Exp.* **4**, 113 (1999).
- [7] M. Rosenbluh, V. Shah, S. Knappe, J. Kitching, *Opt. Exp.* **14**, 15, 6588 (2006).
- [8] J. Kitching, L. Hollberg, A. V. Taichenachev, V. L. Velichansky, V. I. Yudin, *Laser Phys. Lett.* **1**, 10, 257 (2004). G. A. Kazakov, I. E. Mazets, Yu. V. Rozhdestvensky, G. Mileti, J. Delporte, and B. Matisov *Europhys. J. D* **35**, 445 (2005). A. B. Post, Y. -Y. Jau, N. N. Kuzma, W. Happer, *Phys. Rev. A* **72**, 033417 (2005). T. Zanon, S. Guerandel, E. de Clerq, et al., *Phys. Rev. Lett.* **94**, 193002 (2005). G. Kazakov, B. Matisov, I. Mazets, G. Mileti, J. Delporte, *Phys. Rev. A* **72**, 063408 (2005).
- [9] A. V. Taichenachev, V. I. Yudin, V. L. Velichansky, S. A. Zibrov, *Pis'ma ZhETF* **82**, 449 (2005).
- [10] R. Wynands, A. Nagel, S. Brandt, D. Meschede, A. Weis, *Phys. Rev. A* **58**, 196 (1998).
- [11] S. Knappe, M. Stähler, C. Affolderbach, A. V. Taichenachev, V. I. Yudin and R. Wynands, *Appl. Phys. B* **76** 1 57-63 (2003).
- [12] M. D. Lukin, S. F. Yelin, M. Fleischhauer, M. O. Scully, *Phys. Rev. A* **60**, 3225 (1999).
- [13] D. V. Kosachev, B. G. Matisov, Yu. V. Rozhdestvensky, *J. Phys. B* **25**, 2473 (1992).
- [14] E. A. Korsunsky, N. Leinfellner, A. Huss, S. Balushev and L. Windholz, *Phys. Rev. A* **59**, 2302 (1999).
- [15] C. Affolderbach, S. Knappe, R. Wynands, A. V. Taichenachev, V. I. Yudin, *Phys. Rev. A* **65**, 043810 (2002).
- [16] M. J. McDonnell, D. N. Stacey, A. M. Steane, *Phys. Rev. A* **70**, 053802 (2004).
- [17] D. D. Yavuz, *Phys. Rev. A* **75**, 031801(R) (2007).
- [18] G. A. Kazakov, B. G. Matisov, I. E. Mazets, and Yu. V. Rozhdestvensky. *Technical Physics*, **32**, 1414 (2006). A. V. Taichenachev, V. I. Yudin, et al., *Phys. Rev. A* **67**, 033810 (2003).
- [19] D. V. Kosachev *Quant. Electr.* **25**, 11, 1089-1094 (1995).
- [20] P. Violino, *Nuovo Cimento* **6**, 440 (1968).
- [21] I. E. Mazets and B. G. Matisov. *Sov. Phys. JETP* **74**, 13 (1992).
- [22] D. A. Varshalovich, A. N. Moskalev, V. K Khersonskii, *Quantum Theory of Angular Momentum*. World Scientific, Singapore (1988).
- [23] L. D. Landau, E. M. Lifshitz, Vol. 3. *Quantum mechanics, non-relativistic theory*. Pergamon (1991).
- [24] R. H. Dicke, *Phys. Rev.* **89**, 2, 472 (1953).
- [25] C. Affolderbach, A. Nagel, S. Knappe, C. Jung, D. Wiedenmann, R. Wynands *Appl. Phys. B* **70**, 407-413 (2000).
- [26] G. Wasik, W. Gawlik, J. Zachorowski, and W. Zawadzki, *Appl Phys. B* **75**, 613-619 (2002).
- [27] B. J. Dalton and P. L. Knight, *J. Phys. B: At. Mol. Phys* **15**, 3997-4015 (1982).
- [28] M. V. Romalis, E. Miron, G. D. Cates, *Phys. Rev. A* **56**, 6, 4569-4577 (1997).